Fluid Flows Involving a Compound Multiphase Droplet

Prabir Daripa and D. Palaniappan

Department of Mathematics, Texas A&M University

College Station, TX 77843, e-mail: prabir.daripa@math.tamu.edu

Abstract

We present exact analytical solutions for steady-state axisymmetric creeping flows of a viscous incompressible fluid in the presence of a compound multiphase droplet. The solutions given here explain the droplet-fluid interactions in complex situations. The two spherical surfaces constituting a vapor-liquid compound droplet are assumed to overlap with a contact angle $\pi/2$. It is further assumed that the surface tension forces are sufficiently large so that the interfaces have uniform curvature. The singularity solutions for the extensional and stokeslet induced flows in the presence of a compound droplet are deduced from general results. The features of the flow fields and the drag depend on various parameters involved in the problem. In the case of a flow induced by a pair of opposite stokeslets, the streamlines in the continuous phase display toroidal eddy patterns. The eddy changes its size and shape if the locations of the initial stokeslets are altered. These observations may be useful in the study of hydrodynamic interactions of droplets with other objects in a viscous fluid. We also provide a brief discussion of our results in connection with the computation of mobility functions. The exact results presented here can be useful in validating numerical algorithms and codes on multiphase flow and fluid-droplet interactions.

1 Introduction

In recent years, there has been a general surge of interest in understanding the behavior of compound multiphase drops as a result of their occurrence in a variety of engineering systems. These drops occur in processes such as melting of ice particles in the atmosphere, liquid membrane technology as well as in other industrial operations. Gas-liquid compound drops are also found as transient configurations during rapid evaporations of drops near the super heat limit [9] and disruptive combustion of free droplets of multi-component fuels [4]. The studies concerning the lipid bilayer [2] and polymer grafted [1] membranes in concentrated solutions also reveal the existence of compound drops. The experimental evidences recorded in those studies initiated the relevant theoretical investigations in the last few decades.

Some perspectives on the theoretical fluid mechanics of multiphase droplets are discussed in Sadhal et. al. [8]. The compound drop is usually modeled as two overlapping spherical

surfaces with a contact angle. This model has been used in the electric field-induced cell-to-cell fusion process to predict the fusion of biological cells [11]. In hydrodynamics, similar models have been employed to analyze the flow fields in and around a compound droplet [10, 5, 6, 7]. In [10], the translation of a vapor-liquid compound drop was solved by the use of toroidal frame. The expressions for the flow fields and hydrodynamic force were obtained in terms of a rather complicated conical functions. For the overlapping spheres with a contact angle $\pi/2$, simple singularity solutions for the Stokes flow past an encapsulated droplet (compound drop) were presented later in [5]. This simple approach has been further exploited more recently in [6, 7] to derive solutions for a compound drop suspended in complicated flow fields. The analyses provided in the latter articles are the basis for the present study.

In the present analysis we discuss few flow properties concerning droplet-fluid interactions in complex flow situations. In particular, we provide singularity solutions for some axisymmetric flows in the presence of a compound droplet which describe the flow fields in the continuous and dispersed phase fluid regions, respectively. The flow patterns displayed here explains the flow behavior in and around a compound droplet suspended in extensional and stokeslet induced flows. The plots of drag force acting on the droplet illustrate several interesting features. The calculations of the present study can provide the basis for computing mobility functions. It is worth mentioning here that one of the primary motivations behind this work has been to provide exact solutions to somewhat complicated, yet analytically tractable, problems that can be used to validate numerical algorithms and codes on multiphase flow and fluid-droplet interactions.

2 Geometry of the compound droplet

The two-sphere geometry of the compound droplet is depicted in Fig. 1. This geometry consists of two unequal overlapping spheres S_a and S_b of radii a and b with centers O and O' respectively. We assume that these spheres intersect orthogonally. The boundary of the droplet is denoted by $\Gamma = \Gamma_a \cup \Gamma_b$, where Γ_a is part of the boundary where $r = a$ and Γ_b is part of the boundary where $r = b$ (see Fig. 1). Since the spheres overlap at a contact angle $\pi/2$, the two centers share a common inverse point D. In the right-angled triangle OAO', $c^2 = a^2 + b^2$, where $OO' = c$. In the meridian plane, the line AB intersects OO' at D. Hence, $OD = a^2/c$ and $DO' = b^2/c$. Let $(r, \theta, \phi), (r', \theta', \phi)$ and (R, Θ, ϕ) be the spherical polar coordinates of any point outside the assembly Γ with O, O' and D as origins respectively. The geometrical relations that follow from Fig. 1 are given in [6].

Part of the sphere S_b contains a liquid with viscosity different from the viscosity of the liquid around the droplet, and part of the sphere S_a contains vapor. It should be remarked

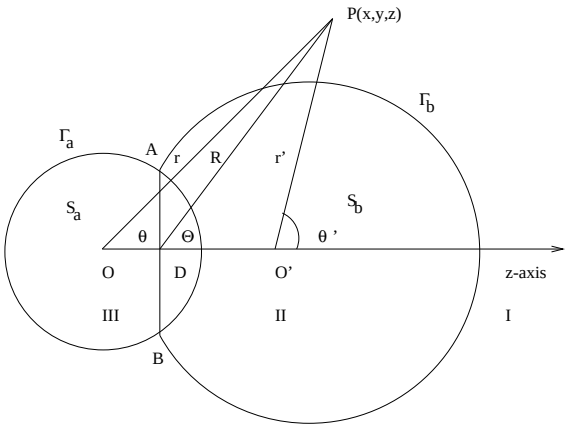

Figure 1: Schematic of a vapor-liquid compound droplet Γ

that the interface separating the vapor and the dispersed phase liquid joins points A and B, and is not the the line AB shown in the Fig. 1. This interface between the phases is assumed to have a uniform curvature different from that of the spheres S_a and S_b. We designate the fluid region exterior to Γ as I and the spherical regions S_b and S_a as II and III respectively. The surface tension forces are assumed to be large enough to keep the interfaces in a spherical shape. The vapor-liquid configuration exists at rest with contact angle approximately 90^o if $\gamma_{I,II} \approx \gamma_{II,III} >> \gamma_{I,III}$ which is in agreement with the Laplace law on all interfaces. Here the $\gamma_{a,b}$ denotes the surface tension at the interface separating regions a and b.

3 Formulation of the Problem

We consider a stationary compound drop submerged in an arbitrary axisymmetric flow of a viscous fluid. The Reynolds number of the flow fields is assumed to be small so that all inertial effects are negligible. In this case, the governing equations for fluid flow are the linearized steady Navier-Stokes equations, also called creeping flow equations or Stokes equations,

$$\mu^{(i)}\nabla^2\mathbf{q^{(i)}} = \nabla p^{(i)}, \quad \nabla\cdot\mathbf{q^{(i)}} = 0, \tag{1}$$

where $i = 1, 2$ refers to continuous and dispersed phase liquids respectively, $\mathbf{q^{(i)}}, p^{(i)}$ and $\mu^{(i)}$ are the velocities, pressures and viscosities in the respective phases. The boundary and interface conditions are as follows: (i) velocity and pressure far from the droplet are that of basic flow; (ii) zero normal velocity on Γ; (iii) continuity of tangential velocity and shear stress at the liquid-liquid interface Γ_b; and (iv) zero shear-stress at the vapor-liquid interface Γ_a. The governing Stokes equations subject to the above far-field and interface conditions constitute

a well-posed problem whose solution provides the velocities and pressures prevailing in the presence of the compound droplet.

As the flow is axially symmetric about the $z-$axis, it is convenient to use the Stokes stream function formulation which requires the solution of the fourth-order scalar equation

$$L_{-1}^2\psi = 0, \tag{2}$$

where L_{-1} is the axisymmetric Stokes operator given by

$$L_{-1} = \frac{\partial^2}{\partial r^2} + \frac{1-\eta^2}{r^2}\frac{\partial^2}{\partial \eta^2}, \tag{3}$$

for the coordinates (r, θ) with $\eta = \cos\theta$. Now the velocity components in terms of the stream function are given by

$$q_r^{(i)} = \frac{1}{r^2\sin\theta}\frac{\partial \psi^{(i)}}{\partial \theta}, \quad q_\theta^{(i)} = -\frac{1}{r\sin\theta}\frac{\partial \psi^{(i)}}{\partial r}, \tag{4}$$

and the pressure is obtained from

$$\frac{\partial p^{(i)}}{\partial r} = -\frac{\mu^{(i)}}{r^2\sin\theta}\frac{\partial}{\partial\theta}(L_{-1}\psi^{(i)}), \quad \frac{\partial p^{(i)}}{\partial \theta} = \frac{\mu^{(i)}}{\sin\theta}\frac{\partial}{\partial r}(L_{-1}\psi^{(i)}). \tag{5}$$

The boundary and the interface conditions stated at the beginning of this section can also be expressed in terms of the stream function (see [6] for details).

4 Results

The solutions for the above problem for various axisymmetric underlying flows are obtained here by the method of images. Since the two spheres intersect at a contact angle $\pi/2$, it is easy to see that the solutions are arrived at the third reflection. The solutions are conveniently represented in cylindrical coordinates if we define $(\rho, \phi, z), (\rho', \phi, z')$ and (Π, ϕ, Z) as the cylindrical polar coordinates with respect to O, O' and D as origins, respectively (see Fig. 1).

Let $\psi_0(\rho, z)$ is the free-space stream function for an axisymmetric motion of a viscous fluid whose singularities lie outside a two-sphere with boundary Γ formed by two unequal spherical surfaces intersecting orthogonally. We also require that $\psi_0(\rho, z) = o(r^2)$ as $r \to 0$. When a compound droplet is introduced in the place of the two-sphere geometry in this flow field ψ_0, the modified stream functions due to the droplet become

$$\begin{aligned}
\psi^{(1)}(\rho, z) &= \psi_0(\rho, z) - \frac{r^3}{a^3}\psi_0\left(\frac{a^2}{r^2}\rho, \frac{a^2}{r^2}z\right) \\
&+ \Lambda\left[\left(\frac{r'(r'^2-b^2)}{2b^3} + \frac{r'^2(r'^2-b^2)}{b^3}\frac{\partial}{\partial r'} - \frac{r'^2(r'^2-b^2)^2}{4b^5}L_{-1}r'\right)\Psi\right] \\
&- (1-\Lambda)\left(-\frac{r'^3}{b^3}\Psi\right),
\end{aligned} \tag{6}$$

for the continuous phase and

$$\psi^{(2)}(\rho,z) = (1-\Lambda)\frac{(r'^2-b^2)}{2b^2}\left[-3+2r'\frac{\partial}{\partial r'}-\frac{(r'^2-b^2)}{2}L_{-1}\right]\left(\psi_0(\rho,z)-\frac{r^3}{a^3}\psi_0(\frac{a^2}{r^2}\rho,\frac{a^2}{r^2}z)\right), \tag{7}$$

for the dispersed phase respectively. The function Ψ in equation (6) is defined as

$$\Psi = \psi_0(\frac{b^2}{r'^2}\rho', c+\frac{b^2}{r'^2}z') - \frac{c^3R^3}{a^3r'^3}\psi_0(\frac{a^2b^2}{c^2R^2}\Pi, \frac{a^2}{c}-\frac{a^2b^2}{c^2R^2}Z),$$

and $\Lambda = \frac{\mu^{(2)}}{\mu^{(1)}+\mu^{(2)}}$. It is easy to show that the expressions (6) and (7) satisfy equation (2) as well as the boundary conditions [7]. The required velocity and pressure fields are computed from (4)-(5). In a similar fashion, the hydrodynamic force acting on the compound droplet is evaluated which is given by

$$\begin{aligned}\mathbf{F} &= 4\pi\mu^{(1)}\left\{[a\mathbf{q}_0]_O + (1-\Lambda)\left([b\mathbf{q}_0]_{O'} - [\frac{ab}{c}\mathbf{q}_0]_D\right)\right\} \\ &+ 6\pi\mu^{(1)}b\Lambda\left\{[(\mathbf{q}_0+\mathbf{q}_{0a})]_{O'} + \frac{b^2}{6}\left[\nabla^2(\mathbf{q}_0+\mathbf{q}_{0a})\right]_{O'}\right\},\end{aligned} \tag{8}$$

where $\mathbf{q}_{0a} = -\text{curl}\left(\hat{e}_\phi\frac{r^3}{a^3}\psi_0(\frac{a^2}{r^2}\rho,\frac{a^2}{r^2}z)\right)$, $\hat{e}_\phi$ being the unit vector in azimuthal direction. The subscripts inside the square brackets in (8) indicate the unbounded flow while the subscripts outside indicate the values of the quantities at those points. The expression (8) represents the Faxen-relation for a compound droplet in axisymmetric flows.

In the following we present singularity solutions for extensional and stokeslet induced flow fields in the presence of a compound multiphase droplet using (6)-(7). The flow due to a stokeslet is an example belonging to the class of singularity induced flows. We also compute the drag on the droplet in each flow.

4.1 Extensional flow past a compound droplet

Here the axisymmetric flow in which the stationary compound droplet is immersed is given by $\psi_0 = \alpha r^3\sin^2\theta\cos\theta$, where α is a shear constant and θ, unless otherwise mentioned below, refers to the polar angle measured counterclockwise at O from the axis of symmetry of the droplet as shown in Figure 1. It is worth pointing out that if the angle θ is measured with respect to a different origin along the axis, then the ψ_0 as given above will correspond to a different extensional flow. Therefore this stream function ψ_0 can be used to refer to several extensional flows simply shifting the point O for the purposes of measurement of angle θ. The exact solutions for this problem can be obtained by the use of (6) and (7). The solution

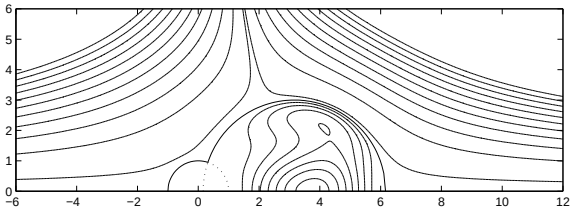

Figure 2: Flow patterns for extensional flow around a vapor-liquid compound droplet.

for the continuous phase is

$$\begin{aligned}
\psi^{(1)}(r,\theta) &= \alpha\rho^2 z - \alpha a^3\frac{\rho^2 z}{r^3} + \Lambda\left[\left(-\frac{5b^3}{2}\frac{z'}{r'}\right.\right.\\
&+ \left.\left.\frac{3b^5}{2}\frac{z'}{r'^3} - \frac{3bc}{2}r' + \frac{b^3 c}{2r'}\right)\alpha\frac{\rho'^2}{r'^2}\right]\\
&- (1-\Lambda)\left[\alpha b^3\frac{\rho'^2 z'}{r'^3} + \alpha bc\frac{\rho'^2}{r'}\right]\\
&+ \Lambda\left[\frac{3a^5 b}{2c^4}R - \frac{a^3 b^3}{2c^3}\left(9\frac{a^2}{c^2} - 2\right)\frac{Z}{R} - \frac{a^5 b^3}{2c^4 R}\left(3\frac{a^2}{c^2} - 2\right)\right.\\
&+ \left.\frac{3a^5 b^5}{c^6}\frac{Z^2}{R^3} + \frac{3a^7 b^5}{2c^7}\frac{Z}{R^3}\right]\alpha\frac{\Pi^2}{R^2}\\
&+ (1-\Lambda)\left[\frac{a^3 b}{c^2}R - \frac{a^3 b^3}{c^3}\frac{Z}{R}\right]\alpha\frac{\Pi^2}{R^2}, \qquad (9)
\end{aligned}$$

and the solution for the dispersed phase is

$$\psi^{(2)}(r,\theta) = (1-\Lambda)\frac{(r'^2 - b^2)}{2b^2}\left[-3 + 2r'\frac{\partial}{\partial r'} - \frac{(r'^2 - b^2)}{2}L_{-1}\right](r^3 - a^3)\alpha\frac{\rho^2 z}{r^3}, \qquad (10)$$

where L_{-1} is defined as in (2). The image system in the continuous phase consists of stokeslets, stresslets, degenerate stokes-quadrupoles and degenerate stokes octupoles located at O and D plus a stokes-quadrupole located at D. It is noticed that the strengths of these image singularities depend on radii of the two spherical surfaces a, b, the distance between the centers c and the non-dimensional viscosity ratio Λ. Some typical flow patterns inside and outside the compound droplet are shown in Fig. 2. There appears to be a circulatory flow in the dispersed phase as seen from Fig. 2.

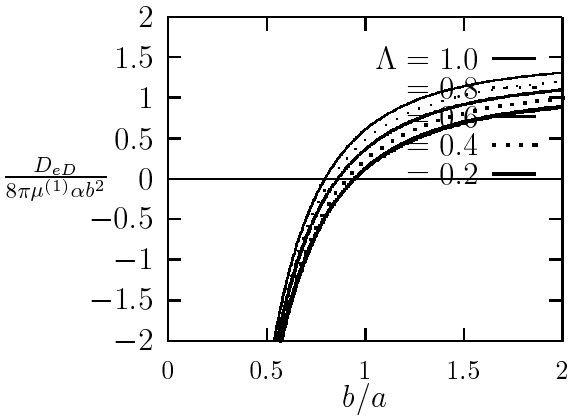

Figure 3: Drag force in extensional flow with origin at D, the center of the circle of intersection of two spheres

The drag force can be calculated using (8). The drag D_e, the force acting in the z direction, in the present case is then found to be

$$\frac{D_e}{8\pi\mu^{(1)}\alpha b^2} = \frac{\beta'}{\beta}\left[\frac{3\Lambda}{2}\left(1-\frac{1}{\beta'^5}\right)+(1-\Lambda)\left(1-\frac{1}{\beta'^3}\right)\right]. \tag{11}$$

We see that the drag force depends on many parameters such as $\beta = \frac{b}{a}$, the distance $c = a\sqrt{(1+\beta^2)} = a\beta'$ between the centers, rate of shear α, and the viscosity parameter Λ. This drag perhaps arises due to the geometrical asymmetry. This geometrical asymmetry vanishes in the limiting cases: (i) $a = 0, b > 0$; and (ii) $b = 0, a > 0$. In these limiting cases, we expect the drag to be zero provided the origin about which θ is measured (see Figure 1) is at the center of the sphere. In fact, we see from (11) that this drag force is indeed zero for $b = 0$ as expected. However, it is non-zero for $a = 0$ because the origin shifts in the this case and is no more at the center of the sphere. It is interesting that the drag in extensional flow significantly depends on the choice of the origin. We shall now illustrate this by choosing the origin at D i.e., at the center of the contact circle. The governing differential equations are the same as they are invariant under translation of origin and the complete solutions can be derived by the use of (6)-(7). It can be seen that the shift of origin strongly influences the strength of primary image singularities such as stokeslet, stresslet and potential-doublet and further introduces an extra stokeslet at O. The higher order singularities however remain unaffected. For the sake of brevity we omit the details and focus our attention on the expression for the drag which is found to be

$$\frac{D_{eD}}{8\pi\mu^{(1)}\alpha b^2} = \frac{\beta}{\beta'}\left[1-\frac{1}{\beta^3}+\frac{\Lambda}{2\beta'^3}\left(\beta'^3+2\right)\right], \tag{12}$$

where the second suffix D indicates that the origin is taken at this point. Clearly, equations (11) and (12) are quite different and interestingly the latter reveals the existence of zero drag corresponding to equilibrium. We observe that the shifting of origin alone does not make the drag zero. Rather, the equilibrium position (for which the force vanishes) depends on the viscosity and radii ratios. The plots shown in Fig. 3 further illustrates these features. The various values for which the force vanishes may be obtained by equating (12) to zero which yields the following relation between viscosity parameter Λ and ratio of radii parameter $\beta = b/a$.

$$\Lambda = \frac{2\beta'^3(1-\beta^3)}{\beta^3(\beta'^3+2)}. \tag{13}$$

The above expression yields the critical value β_c of β for which the drag vanishes at a specified value of Λ. Since Λ lies between 0 and 1, equation (13) gives the constraint $\beta_c \leq 1$ or equivalently $b \leq a$. This in turn implies that the liquid volume should be less than the vapor volume in order to have a vanishing drag force. It also follows from equation (13) that β_c is an increasing function of Λ (see Fig. 3) with $\beta_c = 0.7965595828$ for $\Lambda = 1$ and $\beta_c = 1$ for $\Lambda = 0$. In other words, when the sphere S_b is also a vapor($\Lambda = 0$), the drag becomes zero if the two radii of the spheres are equal which corresponds to the case of composite bubbles. Due to the added symmetry about the plane of intersection in this case, one would expect this result to be true even for the case of arbitrary contact angle. For the vapor-solid assembly ($\Lambda = 1$), the force vanishes when $b/a = 0.7965595828$.

It is also of interest to analyze the stability of the equilibrium (zero drag) position found above. We first observe that in extensional flow the equilibrium results even in the absence of buoyant force and equation (13) gives the values of Λ and β corresponding to equilibrium for which the drag force vanishes. The stability of this zero drag position can be analyzed by moving the origin along $z-$direction. We noticed in the beginning of this section that the shifting of origin along $z-$axis changes the drag force significantly. It can be seen from (11) and (12) that for a given equilibrium value of Λ and β with $\alpha > 0$, moving the origin towards O results in a drag force along positive $z-$direction. Similarly it can be shown that moving the origin towards O' leads to a drag force along negative $z-$direction. Therefore, the equilibrium in this case is clearly stable. For the same equilibrium values of Λ and β with $\alpha < 0$, a similar examination shows unstable equilibrium.

4.2 Stokeslet outside Γ

Here the underlying flow is induced by a stokeslet. We apply the results (6)-(8) to derive the modified flowfield in the presence of a compound droplet.

We consider a stokeslet of strength $\frac{D_3}{8\pi\mu^{(1)}}$, located at a point $(0, 0, c+d)$, say E_1, outside

Γ. The free-space stream function due to this stokeslet is $\psi_0(\rho,z)=\frac{D_3}{8\pi\mu^{(1)}}\frac{\rho_1^2}{r_1}$, where (ρ_1,z_1) are the cylindrical coordinates with E_1 as origin. The flow fields in the presence of the two-sphere assembly with a stokeslet outside it can be obtained by the use of (6) and (7). For the continuous phase, we obtain

$$\begin{aligned}
\psi^{(1)}(\rho,z) &= \frac{D_3}{8\pi\mu^{(1)}}\frac{\rho_1^2}{r_1}-\frac{D_3}{8\pi\mu^{(1)}}\frac{a}{c+d}\frac{\rho_2^2}{r_2}+\frac{D_3}{8\pi\mu^{(1)}}\Lambda\Bigg[-\frac{b}{2d}\left(3-\frac{b^2}{d^2}\right)\frac{\rho_3^2}{r_3}\\
&+ \frac{b^3\left(d^2-b^2\right)^2}{2d^5}\frac{\rho_3^2}{r_3^3}-\frac{b^3\left(d^2-b^2\right)}{(d^4}\frac{\rho_3^2 z_3}{r_3^3}\Bigg]-\frac{D_3}{8\pi\mu^{(1)}}(1-\Lambda)\frac{b}{d}\frac{\rho_3^2}{r_3}\\
&+ \frac{D_3}{8\pi\mu^{(1)}}\Lambda\Bigg\{\left[\frac{ab}{2(b^2+cd)}\left(3-\frac{b^2(c+d)^2}{(b^2+cd)^2}\right)\right]\frac{\rho_4^2}{r_4}\\
&- \frac{a^3b^3(d^2-b^2)(c+d)}{(b^2+cd)^4}\frac{\rho_4^2 z_4}{r_4^3}-\frac{a^5b^3(d^2-b^2)^2}{2(b^2+cd)^5}\frac{\rho_4^2}{r_4^3}\Bigg\}\\
&+ \frac{D_3}{8\pi\mu^{(1)}}(1-\Lambda)\frac{ab}{b^2+cd}\frac{\rho_4^2}{r_4}, \qquad (14)
\end{aligned}$$

and for the dispersed phase, we have

$$\psi^{(2)}(\rho,z)=(1-\Lambda)\frac{(r'^2-b^2)}{2b^2}\frac{D_3}{8\pi\mu^{(1)}}\left[-3+2r'\frac{\partial}{\partial r'}-\frac{(r'^2-b^2)}{2}L_{-1}\right](\frac{\rho_1^2}{r_1}-\frac{a}{c+d}\frac{\rho_2^2}{r_2}), \qquad (15)$$

where $(\rho_2,z_2),(\rho_4,z_4),(\rho_4,z_4)$ are the cylindrical polar coordinates of a point with E_2,E_3,E_4 as origins respectively, and $r_j=r^2-2OO_jr\cos\theta+OO_j^2, j=1,2,3,4$. Here $OO_1=c+d, OO_2=\frac{a^2}{c+d}, OO_3=\frac{b^2+cd}{d}$ and $OO_4=\frac{a^2d}{b^2+cd}$ respectively. Note that E_2 and E_3 lie inside the spheres S_a and S_b respectively, but outside the overlap region and the point E_4 lies inside the overlap region. The image singularities are now located at these points (i.e., at E_2,E_3 and E_4). In contrast to the previous example, the image points are now shifted away from the centers O,O' and their common inverse point D. It is clear that the locations of the image points are indeed dictated by the location of the initial stokeslet. Now the image system in the continuous phase consists of stokeslets at E_2,E_3 and E_4, Stokes-doublets at E_3 and E_4 and Degenerate Stokes-quadrupoles at E_3 and E_4. The strengths of the image singularities depend on radii, the location of the initial stokeslet and the viscosity ratio. It is interesting to note that the image system for a stokeslet near a viscous drop also has the same type of singularities (with different strengths) as the compound drop. But the location of the image singularities in the former is at a single point.

Below we present the flow patterns for the case when the droplet is placed between two stokeslets of opposite strengths. We use the terminology "two opposite stokeslets" to refer to two stokeslets: one with the positive strength, and the other with equal but negative strength. We choose the one which is on the vapor side to have positive strength and the

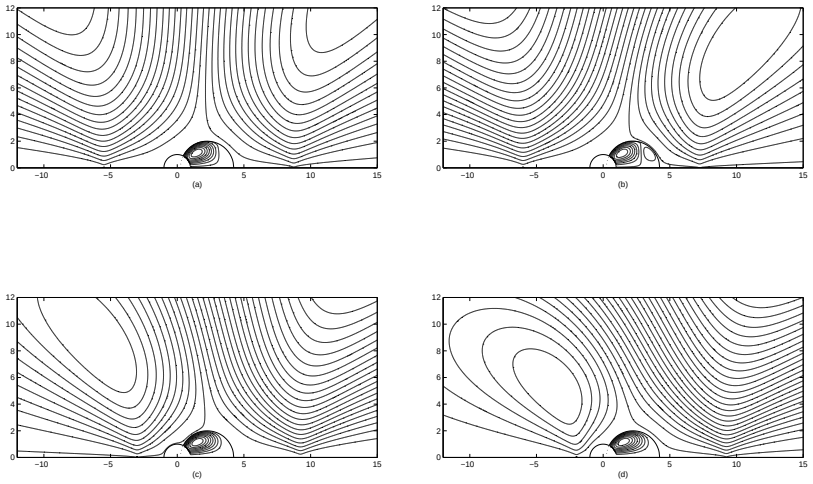

Figure 4: Flow patterns for a pair of opposite stokeslets with $a = 1$, $b = 2$, $\Lambda = 0.6$. (a) $d_b = b + 5, d_a = a + 5$, (b) $d_b = b + 3$, $d_a = a + 5$; (c) $d = b + 5$, $d_a = a + 2$; (d) $d = b + 5$, $d_a = a + 1$. Here d_b, d_a denote the locations of the stokeslets from the liquid and vapor spherical surfaces, respectively.

other on the liquid side to have an equal but negative strength. Fig. 4(a)-(d) shows the flow patterns for the case of two opposite stokeslets for various locations. If the two stokeslets are far from the droplet, the interaction of the stokeslets is not stronger in the neighborhood of the droplet (see Fig. 4(a)). When they are moved closer, a single toroidal eddy structure appears in front of the liquid sphere. This eddy moves further close to the droplet as the stokeslets are moved nearer to the compound drop. We notice that the size and shape of these closed streamlines also change due to the stokeslets moving closer to the droplet. The drag force on the compound droplet, found using (8), is

$$\begin{aligned} \mathbf{F} &= D_3\hat{e}_z\left\{\frac{a}{c+d}+\Lambda\left[\frac{b}{2d}\left(3-\frac{b^2}{d^2}\right)-\frac{ab}{2(b^2+cd)}\left(3-\frac{b^2(c+d)^2}{(b^2+cd)^2}\right)\right]\right. \\ &+ \left.(1-\Lambda)\left[\frac{b}{d}-\frac{ab}{b^2+cd}\right]\right\}. \end{aligned} \tag{16}$$

Here $\mathbf{F} = (F_x, F_y, F_z)$. It can be seen from (16) that the drag force on the compound drop in a stokeslet flow depends on the viscosity ratio, the radii and the location of initial stokeslet. We discuss briefly the variation of drag force with these parameters. In Fig. 5(a) we have plotted $\frac{F_z}{D_3}$ against the location of the stokeslet d for different viscosity ratios with $a = 1$ and $b = 2$. The drag decreases monotonically with increasing values of d as expected. This means that the droplet experiences greater resistance in stokeslet flow if the stokeslet is closer

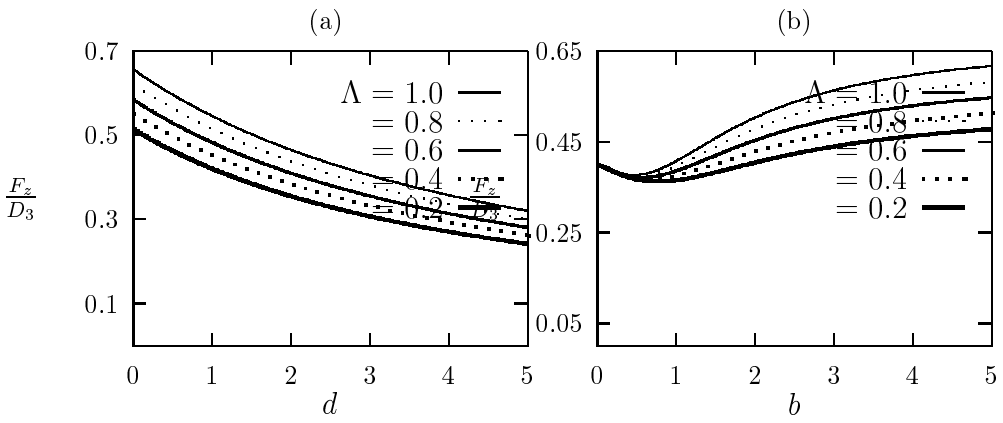

Figure 5: Drag force in a (single) stokeslet flow. (a) Variation with the stokeslet location d for a fixed $a = 1, b = 2$; (b) Variation with the liquid sphere radius b for a fixed $a = 2, d = b + 1$.

to it. Fig. 5(b) shows variation of the drag force with radius 'b' when the stokeslet is at a distance $d = 1$. In this case, the drag force decreases until $b \approx 0.5$ and then starts increasing with increasing values of b. This, in turn, implies that the resistance is greater when the liquid volume is large compared to the vapor volume. It may be noticed that the drag force in general lies between the vapor-solid and vapor-vapor assembly limits. When $\Lambda = 1$, the expression (16) yields the force on a vapor-solid assembly while for $\Lambda = 0$, it reduces to the drag force on a vapor-vapor assembly (composite bubble).

4.3 Mobility functions

The image solutions for Stokes singularities may be employed in a method of reflections type of calculation for the interactions between a compound drop and an arbitrary small particle. The key idea is that over length scales associated with the compound drop, the disturbance fields produced by a small particle may be approximated by those produced by equivalent Stokes singularities (stokeslet, degenerate stokes-quadrupole etc.). In the reflections at the small sphere we can truncate the multipole expansion at the desired order in a_1/c_1, where a_1 is the radius of the smaller particle and c_1 is the distance between the location of the small particle and the center of the compound drop. For reflections at the large sphere, we retain the entire multipole solution, which of course is the image systems of the Stokes singularities. The mobility functions may then be computed in the same way as explained in [3]. The complete calculations of the mobility functions and the hydrodynamic interactions will be discussed elsewhere.

5 Acknowledgment

This research has been partially supported by the interdisciplinary research program of the Office of the Vice President for Research and Associate Provost for Graduate Studies under grant IRI-98.

References

[1] Evans, E., Klingenberg, D. J., Rawicz, W., & Szoka, F. 1996 Interactions between polymer-grafted membranes in concentrated solutions of free polymer. Pre-print.

[2] Evans, E., & Needham, D. 1988 Attraction between lipid bilayer membranes in concentrated solutions of non-adsorbing polymers: Comparison of mean-field theory with measurements of adhesion energy. *Macromolecules* **21**, pp. 1822-1831.

[3] Kim, S. & Karrila, S. J. 1991 Microhydrodynamics: Principles and Selected Applications. Boston: Butterwort-Heinemann.

[4] Lasheras. J. C., Fernandez-pello, A. C., & Dryer, F. L. 1980 Experimental observations on the disruptive combustion of free droplets of multicomponent fuels. *Combust. Sci. Technol.,* **22**, pp. 195-209.

[5] Palaniappan, D. & Kim, S. 1997 Analytic solutions for Stokes flow past a partially encapsulated droplet. *Phys. Fluids* **A9(5)**, pp. 1218-1221.

[6] Palaniappan, D. & Prabir Daripa. 2000 Compound droplet in extensional and paraboloidal flows. *Phys. Fluids*, **12(10)**, pp. 2377-2385.

[7] Prabir Daripa, & Palaniappan, D. Arbitrary axisymmetric creeping flows in and around a compound droplet. *Phys. Fluids* (submitted).

[8] Sadhal, S. S., Ayyaswamy, P. S., & Chung, J. N. 1997 Transport Phenomena with Drops and Bubbles. Springer-Verlag, New York.

[9] Shepherd, J. E., & Sturtevant, B. 1982 Rapid evaporation at the super heat limit. *J. Fluid Mech.,* **121**, pp. 379-402.

[10] Vuong, S. T., & Sadhal, S. S. 1987 Growth and translation of a liquid-vapor compound drop in second liquid. Part 1. Fluid Mechanics. *J. Fluid Mech.* **209**, pp. 617-637.

[11] Zimmermann, U., & Vienken, J. 1982 Electric field-induced cell-to-cell fusion. *J. Memb. Biol.* **67**, pp. 165-182.